17

Ultra-Sensitive Optical Atomic Magnetometers and Their Applications

Igor Savukov
Los Alamos National Laboratory
USA

1. Introduction

In this chapter, we overview the most sensitive contemporary atomic magnetometers (AM) that are based on high-density alkali-metal vapors. These magnetometers are considered in a broader content of other magnetometers and their applications. The principles of the operation of the AMs are explained for better understanding of this topic. One point of focus in this chapter which establishes the connection to the title of this book is about the relation between lasers and most sensitive atomic magnetometers. The chapter is organized in the following way. After general introduction to the AMs and the applications of magnetometers, the principles of the operation of optical atomic magnetometers are given. With this background information, next so-called SERF magnetometers and their features are discussed. Then, the discussion continues to the topic about the operation of "SERF magnetometers" in the non-SERF regime. Finally, after covering the principles and theory, we return to some most notable applications of atomic magnetometers.

Since their discovery, lasers have revolutionized many fields – the field of AMs or magnetometers in general is no exception. Before the advent of lasers, AMs were based on discharge lamps which though relatively simple and inexpensive light sources did not provide enough power and had some other drawbacks for the realization of maximum sensitivity that can be achieved with atomic magnetometers. In a comparison of sensitivity of the state-of-the-art Cs magnetometers based on a Cs discharge lamp and a semiconductor laser made in Ref. (Groeger et al., 2005), the lamp Cs magnetometer had sensitivity of 25 $fT/Hz^{1/2}$ that was lower than that of the same but laser-based magnetometer, 15 $fT/Hz^{1/2}$. For most sensitive magnetometers the difference is expected much more significant, although there is no investigation of this question in the literature. From Ref.(Groeger et al., 2005), we can estimate that the intensity of the lamp light in the Cs absorption band was below 1 mW, and such power would be suboptimal in most sensitive magnetometer based on high-density vapors, such as spin-exchange relaxation free (SERF) magnetometer (Allred et al., 2002). The absence of lasers is one of the factors that initially atomic magnetometers had been far behind superconducting quantum interference devices (SQUIDs) in sensitivity.

Although the introduction of lasers into magnetometry improved sensitivity, laser-based magnetometers are not yet commercially available. However, this can change in the near future. Diode lasers of high quality are becoming less expensive, and some lasers such as vertical cavity surface-emitting lasers (VCSELs) in addition to extremely low price allow

Source: Advances in Optical and Photonic Devices, Book edited by: Ki Young Kim,
ISBN 978-953-7619-76-3, pp. 352, January 2010, INTECH, Croatia, downloaded from SCIYO.COM

integration into microfabricated packages. Such packages will be not only inexpensive and easy to batch produce they will also have lower power consumption, light weight and unimpeded mobility (Knappe et al., 2006).

Sensitive magnetic field measurements, for which AMs can be used, are important owing to many existing and potential applications. Magnetometers have been in wide use, for example, in geology, military, biomagnetism, space magnetic field measurements. AMs have been used because they are both relatively sensitive compared to conventional inexpensive magnetometers, such as fluxgates, and more convenient compared to SQUIDs that require cryogenic cooling. For a long time low-T_c SQUIDs had been by far the most sensitive magnetometers at low frequency. However, this has changed with the demonstration with AMs of record 0.5 fT/Hz$^{1/2}$ sensitivity (Kominis et al., 2003).

High-sensitivity AMs are based on spin-polarized atomic gases or vapors, and AM research is closely related to the atomic physics subfield dedicated to the investigation of spin interactions in such media. This subfield includes the research on optical pumping and related topics such as atomic clocks, masers, hyperpolarized gases, spin-based spectroscopy, and some others. A comprehensive review of optical pumping experiments before 1972 and theory of optical pumping and various relaxation mechanisms are given by William Happer (Happer, 1972). This theory, which still stands the test of time, includes the formulation of density matrix equations, which can be directly applied to the analysis of magnetic resonances of vapors on which atomic magnetometers are based. Atomic magnetometers find many applications as other magnetometers, but they are most useful when high sensitivity and non-cryogenic operation are required. For example, AMs have been developed for submarine detection, and many other military applications are possible on similar principles. Some applications of Rb-vapor or ^{3}He magnetometers in geophysics and space physics were mentioned as early as in 1961 by Bloom (Bloom, 1961) who did some pioneering work on the high-sensitivity measurements of magnetic fields and theory for the operation of atomic magnetometers. Theoretical analysis of early atomic magnetometers was also done by Dehmelt (Dehmelt, 1957) and by Bell and Bloom (Bell & Bloom, 1957). Although the history of atomic magnetometers is quite fascinating and they played an important role in applications where simpler and less expensive methods did not provide sufficient sensitivity, the atomic magnetometers of the past were much less sensitive than the modern ones. Most exciting results appeared only recently with the various demonstrations of performance of high-density AMs, which we would like to focus on in this chapter.

2. Principles of operation of sensitive atomic magnetometers

2.1 The interaction of spins with magnetic field

First of all, AMs are based on atomic spins which due to their magnetic moment interact with magnetic field. The Hamiltonian related to this interaction in the formalism of quantum mechanics is

$$H = \gamma_e \mathbf{J}\cdot\mathbf{B} + \gamma_N \mathbf{I}\cdot\mathbf{B} + a_{hf}\mathbf{J}\cdot\mathbf{I}\,, \tag{1}$$

where $\gamma_e = g_J\mu_B/\hbar$, $\gamma_N = g_I\mu_B/\hbar$, μ_B is the Bohr magneton, g_J, g_I are electron's and nuclear g-factors, $\mathbf{J}$ is the total angular momentum of the electron, the sum of the spin and the orbital momentum, $\mathbf{J} = \mathbf{S} + \mathbf{L}$; $\mathbf{I}$ is the nuclear angular momentum, and a_{hf} is the hyperfine

constant. This Hamiltonian is responsible for the splitting of hyperfine sublevels in magnetic field, called the Zeeman splitting. Because in small external field the third term dominates, it is convenient to employ the basis of total momentum of the atom $\mathbf{F} = \mathbf{I} + \mathbf{J}$ for the classification of the hyperfine sublevels. In zero external field the total angular momentum F and its projection M are "good" quantum numbers, but by continuity we can use this classification when $|F, M\rangle$ states are no longer eigenstates of the Hamiltonian (1). The solution of the Schrödinger equation in the presence of magnetic field and hyperfine interaction for the case $\mathbf{J} = \mathbf{S} = 1/2$ is known as the Breit-Rabi equation:

$$W(F, M_F) = -\frac{\Delta W}{2(2I+1)} - \frac{\mu_I}{I} B M_F \pm \frac{\Delta W}{2} \sqrt{1 + \frac{4M_F}{2I+1} x + x^2}\ , \tag{2}$$

where $\Delta W = a_{hf}[F_2(F_2+1) - F_1(F_1+1)]/2$ is the hyperfine splitting between $F_2 = I + 1/2$ and $F_2 = I - 1/2$ states at zero field, $x = (g_J - g_I)\mu_B B / \Delta W$. Fig. 1 shows the dependence of the energy of hyperfine sublevels on applied DC magnetic field. The transitions between magnetic sublevels $M \to M \pm 1$ can be induced by time-varying magnetic interaction $H = \gamma_e \mathbf{J} \cdot \mathbf{B}(t) + \gamma_N \mathbf{I} \cdot \mathbf{B}(t)$ (we can neglect the second term, which is about 3 orders of magnitude smaller). If oscillating field is applied, by scanning its frequency, the Zeeman resonances can be observed, which are also called magnetic resonances. The resonance frequency at small field is directly proportional to the applied DC field. It is also possible to induce transitions between hyperfine levels $F_2 = I + 1/2$ and $F_2 = I - 1/2$ separated by the ΔW gap. These transitions are used in atomic clocks and masers. Because the splitting is quite stable, essentially it is dependent on constant internal field produced by the nucleus, high-quality clocks can be built. One figure of merit for clocks is the Q factor of resonance, and it is very high in the case of hyperfine transitions. Even in atomic vapors, where various collisions damp hyperfine resonances, not to mention traps and atomic fountains, where the collision effects are much smaller, Q factors can exceed 1 million. The Zeeman transitions can also have high Q factors at high frequencies because the resonance width, which is on the order of 1 kHz at high density of vapor and a few Hz at low density in cells with coating, does not change over large frequency range as long as gradients arising from the applied field are not very strong and the field is stable. In comparison to other resonance systems such as mechanical oscillators and LC-resonance circuits, the Zeeman resonances of atomic

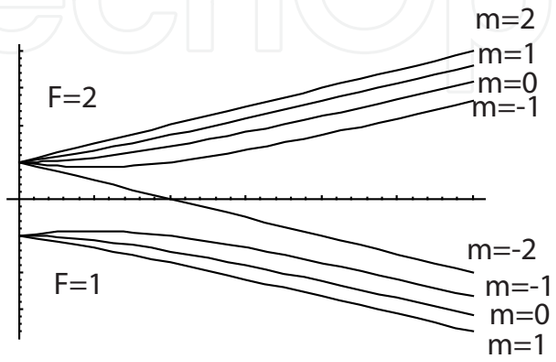

Fig. 1. Dependence of Zeeman sublevels on magnetic field for the case of I=3/2.

magnetometers at sufficiently high frequency can be considered of very high quality. Apart from direct applications in the magnetic field measurements, these resonance properties can be also useful for building radio receivers and filters.

The Zeeman level splitting and transitions between the Zeeman levels under the action of field is the quantum-mechanical picture of the interaction of the field with the spins, which is most appropriate for quantum objects such as atomic spins. However, in practice, the classical picture can be more convenient to use. In the classical picture, the magnetic field causes torque on the spins, and their behavior is described by the Bloch equations:

$$\begin{aligned} dS_x/dt &= \gamma S_y B_z - \gamma S_z B_y - S_x/T_2 \\ dS_y/dt &= -\gamma S_x B_z + \gamma S_z B_x - S_y/T_2 \\ dS_z/dt &= \gamma S_x B_y - \gamma S_y B_x + (S_0 - S_z)/T_1 \end{aligned} \tag{3}$$

Here γ is the gyromagnetic ratio of atomic spins (the slope of the energy-field curve in Fig. 1). In order to account for various relaxation mechanisms, the terms with phenomenological relaxation times T_1 and T_2 are added. T_1 is the longitudinal relaxation time, which shows how fast the spin ensemble reaches equilibrium when spins are oriented along the field, and T_2 is the transverse relaxation time, which characterizes the decay of transverse excitation of spins. The use of the Bloch equations can be justified in certain cases when the number of spins N is so large that quantum fluctuations of spin projections that scale as $1/N^{1/2}$ can be neglected and when resonance frequencies of multiple Zeeman transitions are the same so the majority of spins of various hyperfine levels precess together as the whole. Though very small at these conditions, quantum fluctuations can be added to the Bloch equations for the analysis of fundamental noise of the atomic magnetometer (Savukov et al., 2005). The conditions of collective precession of spins with the same frequency and relaxation times for all Zeeman sublevels are not always satisfied, but in some practically important regimes of operation, the Bloch equations give quite adequate explanations of observed effects. The Bloch equations are also convenient that they provide analogy with NMR, where they are routinely used for the analysis of various schemes for manipulating nuclear spins. NMR-like effects, such as the free-induction decay, spin echo, rf broadening, gradient broadening, exist in atomic magnetometers and can be used in applications. Even when the Bloch equations are not rigorously justified, they can still provide qualitative description of many experiments with atomic magnetometers.

Alternatively, if accurate description is desirable, the density matrix (DM) equation

$$\begin{aligned} \frac{d\rho}{dt} = a_{hf}\frac{[\mathbf{I}\cdot\mathbf{S},\rho]}{i\hbar} + \mu_B g_S \frac{[\mathbf{B}\cdot\mathbf{S},\rho]}{i\hbar} + \frac{\varphi(1+4\langle\mathbf{S}\rangle\cdot\mathbf{S})-\rho}{T_{SE}} + \\ + \frac{\varphi-\rho}{T_{SD}} + R[\varphi(1+2\mathbf{s}\cdot\mathbf{S})-\rho] + D\nabla^2\rho \end{aligned} \tag{4}$$

can be used (Happer, 1972; Appelt et al., 1998; Alred et al., 2002; Savukov & Romalis, 2005). Here ρ is the density matrix, which has dimension of the number of hyperfine states; $\varphi = \rho/4 + \mathbf{S}\cdot\rho\mathbf{S}$ is the pure part of the density matrix, $\langle\mathbf{S}\rangle = Tr(\rho\mathbf{S})$, T_{SE} is the spin-exchange (SE) collision time, T_{SD} is the spin-destruction time, R is the pumping rate, and $\mathbf{s}$ is the optical pumping vector which is oriented in parallel with the direction of the pump beam

and its magnitude and sing depends on the degree of circular polarization. A DM equation is the generalization of Schrödinger equation, normally applicable to pure states, for the case when states are mixed due to collisions between atoms, which cannot be ignored. Some terms (the first and the second) can be directly obtained from the Hamiltonian of the Schrödinger equation via the Von Neumann equation, $i\hbar\frac{d\rho}{dt}=\left[H,\rho\right]$, but others require some non-trivial theoretical derivation. Unlike the Bloch equations where the relaxation and equilibrium polarization were introduced phenomenologically, the DM equation contains explicitly relaxation terms and optical pumping terms that determine the equilibrium polarization. The solution of the DM equation can be used to explain many observed effects in atomic magnetometers, including precession frequency of spins and their relaxation rates in a wide range of experimental conditions, and is considered the most appropriate theoretical framework. Unfortunately, the DM equation has to be solved numerically, and the solutions are cumbersome for the analysis. The solution also takes significant computational time due to non-linear nature of the equation arising from the SE term, $\frac{\varphi(1+4\langle\mathbf{S}\rangle\cdot\mathbf{S})-\rho}{T_{SE}}$. Still in several limits the DM equation can be simplified and some intuitive pictures of spin dynamics can be obtained using for example the method of separation on spin subsystems and perturbation theory. Quite useful separation is on the upper (*F=I+1/2*) and the lower (*F=I-1/2*) hyperfine manifold subsystems of the ground state. In the presence of magnetic field, the upper manifold Zeeman components precess in one direction and the lower manifold components precess in the opposite direction. Thus instead of a single set of Bloch equations (2) two sets of the Bloch equations can be applied separately to these systems of precessing spins:

$$\begin{aligned}\frac{d\mathbf{S}_{up}}{dt}&=\gamma\mathbf{B}\times\mathbf{S}_{up}\\ \frac{d\mathbf{S}_{down}}{dt}&=-\gamma\mathbf{B}\times\mathbf{S}_{down}\end{aligned}\tag{5}$$

A coupling between the oppositely rotating spins exists due to SE collisions, which can lead either to full alignment of two subsystems if the precession frequency is much lower than the rate of SE collisions or to relaxation otherwise. In the former case, a single set of the Bloch equations can be used to describe the precession of the spins.

Another important concept that allows us greatly simplify the analysis is the spin-temperature (ST) distribution. A ST density matrix is $\rho_{ST}=k_n\exp(\boldsymbol{\beta}\mathbf{F})$, where $\boldsymbol{\beta}$ is the ST parameter, k_n is the normalization factor, and $\mathbf{F}$ is the total angular momentum vector. The ST density matrix can be characterized by a single vector – the total spin of the system or polarization vector. The ST distribution for *I=3/2* is illustrated in Fig. 2. By substituting the ST distribution into the DM equation, Eq. 4, we find that it is a solution of this equation. The ST distribution is maintained in the SERF regime in the static and the rotating frame if spins change their orientations slow compared to the SE rate. When the DM has a ST distribution, the SE term does not lead to any relaxation and the spin dynamics is very similar to that described with the Bloch equations in the static or rotating frames. However, beyond the SERF regime, the ST distribution is not strictly valid. Still when the deviation from the SE

distribution is small, perturbation theory can be effectively used to account for this small deviation. One practically important example is the case of small excitation by time-varying magnetic field. The theory of so-called rf magnetometer is based on this approach (Savukov et al., 2005). [See also (Appelt et al., 1998) where detailed solution of the DM equation is given.] It is also possible to apply perturbation theory in some cases of large excitation amplitudes. For example, when spin polarization is large, under condition of strong excitation most spins follow the ST distribution in the rotating frame, and perturbation theory can be used to account for small deviations from this pattern.

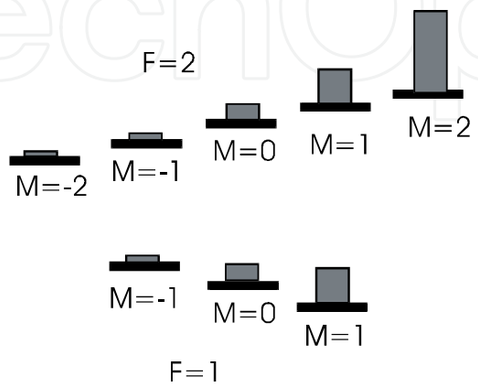

Fig. 2. A spin-temperature distribution

2.2 The interaction of spins with light

The interaction of spins with light leads to a number of phenomena such as optical pumping, dependence of optical properties on spin states, light shift, light-induced spin-destruction, and light narrowing of magnetic resonances that are encountered in atomic magnetometers. Optical pumping, in particular, is an essential feature of high sensitivity atomic magnetometers. In general optical pumping, quite common process in laser physics, leads to redistribution of atomic levels. For example, many lasers are based on population inversion that is created by irradiating laser medium with light. More specifically, in the context of AMs, optical pumping means the redistribution of magnetic sublevels due to absorption of light. Optical pumping can change the total spin of initially disoriented spins and can lead to build up of spin polarization. Although magnetic field prepolarization can be in principle used to create the preferential spin orientation and non-zero magnetometer signal, the optical pumping is much more efficient. It can increase polarization by many orders of magnitude compared to thermal equilibrium values even in strong field. With sufficient pumping power (about 10 mW), the expectation value of spin can reach almost maximum value, which is ½ in the case of S=1/2. For comparison, in NMR, such levels can not be reached with the strongest polarization magnets. Only the combination of high field (10 T) and low, liquid-helium temperature (4 K) can produce similar polarization of electron spins, but this method is not practical especially for alkali-metal vapors that have to be kept at much higher temperature.

Optical pumping of atomic spins can be illustrated and estimated in the case of circularly polarizing light by using the fundamental law of conservation of angular momentum. Circularly polarized photons have spin 1. In the act of absorption, according to this law the photons transfer their spins to atoms. The selection rules is another way to understand this process: the magnetic sublevel M changes by 1 in a transition to the excited state induced by

circularly polarized light, so the expectation value of the atomic spin, which depends on M, changes. From excited states, atoms decay, either spontaneously or through collisions with other atoms, to the ground state. The overall cycle results in the change of angular momentum or spin of the ground state. The efficiency of pumping can be quite high – typically in atomic magnetometers on average only 1.5 photons are required to polarize one alkali-metal atom in the ground state. The described above pumping process is called depopulation pumping, because it is arranged that the photons preferentially depopulate the atomic states of some M with higher probability than others. It is possible to arrange other schemes of optical pumping. Some of them are analyzed in the review paper [Happer 1972]. In optical pumping not only the expectation value of spin (vector) can be changed, but also the expectation values of multipoles of higher order, if the state has angular momentum greater than ½. The terms orientation and alignment are used to differentiate odd and even multipoles or just dipole and quadrupole moments [(Budker et al., 2004), appendix about atomic polarization moments]. For example, if M=-1,0,1 levels are populated in the proportion 1:0:1, the system will have alignment but no orientation. Alignment, as orientation, precesses around magnetic field and can be used for magnetic-field measurements. Sensitive magnetometers based on various multipoles have been explored extensively by D. Budker group at UC Berkeley.

To build a sensitive magnetometer such as SERF, in addition to optical pumping it is necessary to utilize optical probing. Optical probing is a high-sensitivity method to detect the states of atomic spins based on strong spin-dependent interaction of light with polarized atoms. Alternatively, a pick-up coil can be used in some cases, but its sensitivity is low at low frequency. For example, the SERF magnetometer has only frequencies below a few hundred Hz range and a coil will not be very sensitive. The optical probing signal, on the other hand, does not depend much on frequency, and the optical probing can be used for detection of DC fields. The only problem could be 1/f noise, that exists at very low frequencies owing to various reasons. To reduce this technical noise, some methods of modulation can be implemented. For example, a polarization modulator can be inserted into the probe beam path to shift the low-frequency AM signal to frequencies of a few kHz.

The high sensitivity of optical detection is due to both strong interaction of light with spins and high sensitivity of polarization angle measurements (or absorption measurements) that can reach quantum limit of photon fluctuations. This limit is extremely small, on the order of nrad/$Hz^{1/2}$. Note that one nrad is the angular size of a 1-mm object at the distance 1000 km! The interaction of light with atoms is strong because atoms, especially in gas phase, have very narrow optical absorption resonances and large transition amplitudes. For example, alkali-metal atoms of concentration of 10^{14} atoms/cc can absorb resonant light in the path length on the order of 1 mm. Quantitatively, the absorption coefficient α, or the inverse absorption length, can be found from the oscillator strength (f), the density of atoms (n), and the width of absorption profile (γ). In the case when the buffer gas pressure is sufficiently high (which is the case in SERF magnetometers), the hyperfine splitting and Doppler broadening can be neglected, and the absorption coefficient of a specific line, such as D1, becomes a single Lorentzian:

$$\alpha = ncr_e f \frac{\gamma}{(\nu - \nu_0)^2 + \gamma^2}. \tag{6}$$

In the center of the resonance, the absorption coefficient $\alpha = ncr_e f / \gamma$. The absorption coefficient depends on optical linewidth, which in turn depends on the gas composition of the magnetometer cell, buffer gas pressure, if present, and temperature. Buffer gases are frequently added to reduce diffusion to the wall and for other functions, for example, to achieve high spatial resolution of AM measurements. When the potassium cell is filled with He, the linewidth is about 7 GHz (HWHM) or 0.014 nm per 1 amg (1 amg is the density of the gas for 1 atm at normal conditions). This line width at He density on the order of 1 amg exceeds the hyperfine spitting of K (I=3/2), equal to 462 MHz, and Doppler width HWHM=0.5 GHz. In heavier alkali-metal atoms the hyperfine splitting, which is 3036 MHz in Rb (I=5/2) and 9192 MHz in Cs (I=7/2), can become comparable to the buffer gas broadening for the pressures about 1 atm. Thus especially in the case of Cs two-component absorption profile will appear. The absorption coefficient is strong for all buffer gas densities used in SERF magnetometers, up to 10 amg. The optical probing sensitivity is also high in this range of densities.

Both absorption and light polarization rotation (Faraday effect) can be used for detection of spins. In most sensitive magnetometers, such as SERF, light polarization rotation measurements were chosen over absorption measurements. One drawback of the absorption method is that the probe laser has to be tuned close to the center of absorption line, and this leads to stronger spin-destruction as well as to strong attenuation of the probe beam, especially in optically thick high-density vapors. In the Faraday detection method, on the other hand, the probe laser is tuned away from the resonance, which facilitates the propagation of light through optically thick medium and reduces the spin destruction.

According to the rules of optics, the plane of polarization of linearly polarized light will be rotated by non-zero angle

$$\theta = \frac{\pi(n_- - n_+)l}{\lambda} \tag{7}$$

if the refractive indices for right and left circularly polarized light components n_+ and n_- are not equal, where λ is the wavelength and l is the pathlength. This is possible when spin-up and spin-down ground-state levels are unequally populated for quantization axis chosen along the direction of the light propagation. Large rotation of light polarization in optically pumped vapors is due to the strong dependence of refractive index on atomic spin orientation. It can be derived from Eqs.6 and 7 and the Kramers-Kronig relations that the rotation angle by alkali-metal atoms is

$$\theta = \pm\frac{1}{2} l r_e c f n P_x D(\nu - \nu_0) , \tag{8}$$

where $D(\nu)$ is Lorentzian dispersion profile, l is the path length, and r_e is the classical electron radius. This is the expression for the D1and D2 lines, with opposite signs for their contributions.

The rotation of polarization by optically-pumped vapors, which can be evaluated with Eq. 8, exceeds by many orders of magnitude usual Faraday rotation in other substances.

In theory of AMs, the questions about spin-destruction and light shifts by pump and probe beams also arise. The mechanism of light-induced spin-destruction is similar to that of spin

pumping: when light is absorbed it changes the spin states, or in other words perturbs the spins. In the light-induced spin destruction the change in the spin state leads to the loss of coherence and longitudinal polarization. Both circularly polarized and linear polarized light can induce spin destruction, but only circularly polarized component of light builds up the orientation of spins. Hence if the degree of circular polarization is smaller than 1, the maximum polarization level will be less than 1 for arbitrary light intensity. This result can be written as $P = sR/(R + R_{SD})$, where s is the degree of circular polarization and $R_{SD} = 1/T_{SD}$. This coefficient also includes the reduction owing to possibly non-zero angle between the beam direction and the spin orientation, which can be forced away from the beam direction by an applied magnetic field. Scattering of pump light by atoms can also lead to the reduction of the ultimate polarization. However, this effect is minimized in the SERF atomic cells that contain nitrogen buffer gas, which quenches excited states so atoms do not re-emit photons in random directions after the absorption of the pump light.

Light shift is the AC Stark effect, i.e. the shift of atomic energy levels in AC electric field produced by light. An unperturbed atom has zero electric moment (extremely small electric moment might exist, but its effect is hardly detectable), so Stark effect appears only in the second order of perturbation theory in dE term. In other words, electric field polarizes the atom and interacts with the dipole moment of the polarized atom. When light has wavelength in the vicinity of absorption resonance, significant enhancement of AC Stark effect appears due to the reduction of denominator in the perturbation theory. Minimal denominator value is determined by the width of the excited state. On the other hand, AC Stark shifts between Zeeman levels have significant cancellations so they are quite small, but observable since Zeeman resonances are narrow, reaching a few Hz in SERF magnetometers. It also can be shown that light shift [see for detail (Appelt et al., 1998)] is the imaginary part of the complex optical pumping, which can be introduced by replacing absorption Lorentzian with the complex Lorentzian.

Thus the maximum magnitude of light shift is on the order of the pumping rate that will be obtained at the center of the absorption line. Light shift follows dispersion Lorentzian, while the pumping rate follows absorption Lorentzian, both having the same prefactor. Light shift can be expressed in the units of frequency as the pumping rate, but by dividing light-shift frequency by gyromagnetic coefficient, it can also be expressed in the units of magnetic field. Actually, the effect of light shift on the spins is equivalent to that of a magnetic field and it can be included into the Bloch equations or in the density matrix equation on the equal footing as usual magnetic field. However, if there is more than one type of atom in the cell, the light shift "field" will be different for different atoms. The direction of the light-shift "field" is along the direction of the beam and the sign depend on the sign of circular polarization. Circularly polarized light creates light shift, but linear polarization does not except for very small light-shift noise arising from fundamental fluctuations in the difference of the number of photons of two circularly polarized components of which the linearly polarized light is composed.

Light shift is a parasitic effect in AMs which can add noise to the AM signal and lead to the broadening of magnetic resonances. Because light shift depends on the wavelength as the dispersion Lorentzian, it can be minimized by tuning the laser to the center of absorption resonance. However, this cannot be done for the probe beam, which is deliberately tuned

off the resonance to avoid strong absorption. Although the probe beam is linearly polarized, due to imperfections, for example birefringence of glass cell walls, light-shift from the probe beam is always present. By minimizing its intensity, stabilizing wavelength, light shift can be made small and quite constant, so it won't lead to a large noise in the magnetometer.

As we mentioned above, optical pumping and optical probing are essential features of most sensitive AMs. Although it is possible to use very simple light sources for pumping and probing such as discharge lamps, their intensity over the absorption spectrum of atoms used in AMs is not sufficient for reaching best sensitivity and lasers have to be used. A question arises, then, what are requirements for the lasers to be good candidates for AMs? The primary parameter is the wavelength. The wavelength selection depends on the atoms that are used in the magnetometer. Ultra-sensitive magnetometers in order of their sensitivity are based on K, Rb, and Cs vapors. Usually D1 lines of these atoms are preferable, but D2 lines or other lines, which are less convenient from point of view of wavelength availability, in principle can be used. The D1 line ($ns_{1/2}$-$np_{1/2}$, where n=4,5,6 for K, Rb, Cs, respectively) has the advantages over D2 line ($ns_{1/2}$-$np_{3/2}$, the same n) that the pumping on the D1 line by circularly polarized light makes the vapor transparent to this light, so the pump beam can propagate over distances greatly exceeding the (low-intensity) absorption length. The intensity propagation equation for D1 line is $dI / dz = -\alpha(1 - P_z)I$, where I is the intensity and P_z is the polarization projection along the propagation direction z. When P_z is close to 1, the absorption coefficient will be multiplied by a small factor (1- P_z) and hence will be significantly reduced. In addition, as it follows from the solution of the propagation equation, the intensity will be attenuated linearly rather than exponentially, which allows to create a more uniform AM sensitivity across the cell. This is especially important in SERF magnetometers with optical densities exceeding 10. Although it is possible to tune the laser away from the resonance to reduce absorption and allow penetration through the cell for the D2 line, this method will have a drawback of large light shift, discussed earlier, which can introduce noise into the magnetometer signal and broadening owing to non-uniformity of the light shift across the cell. Another advantage of the D1 lines is that optimized magnetometer signal (when the probing is based on the Faraday effect) is two times larger. This advantage is not crucial, and D2 lines still can be used for probing spins especially if the laser of higher quality is easier to find for this line. The optimization of wavelength for each line is done experimentally by tuning the wavelength to maximize the signal or even better SNR. Because the magnetometer signal is the product of the Faraday rotation, which depends on wavelength as the dispersion Lorentzian, and intensity, which is reduced exponentially with absorption coefficient that depend on wavelength as absorption Lorentizian, the maximum of the signal is located a few linewdths from the center of the line. To reduce also spin destruction by the probe light, which has the same wavelength dependence as the absorption coefficient and is proportional to the intensity, the probe laser can be detuned further away than the wavelength of the maximum of the signal and the beam can be expanded to fill out the atomic cell. This can lead to the improvement of SNR. However, if probe light is tuned too far away from the resonance, the opposite rotations by D1 and D2 lines (Eq. 9) can become comparable and cancel each other. This precludes sensitive detection and effective pumping, for which similar cancelation occurs, with broad-spectrum light. If we choose to use the D1 lines because of the described advantages, then

following wavelengths of the pump and probe lasers will be needed: 700 nm for K , 795 nm for Rb , 894.6 for Cs, with some tuning range 0.2 nm allowed for optimization. Many diode lasers of these wavelengths are available, making an AM a quite inexpensive device easy to operate.

In addition to the wavelength selection, the requirement for power is also important to consider. For relatively small cells employed in single-channel magnetometers, the power on the order of 50 mW is sufficient. The pump power requirements can be simply estimated from the analysis of the magnetometer sensitivity as the function of the pumping rate. For example, the signal of the SERF magnetometer scales as $R/(R+R_{SD})^2$ (it is directly proportional to polarization level, which is the ratio $R/(R+R_{SD})$, and inversely to magnetic resonance width or $R+R_{SD}$)and hence the optimal value of the pumping rate is $R=R_{SD}$. If the pumping rate is below this value, the signal linearly decreases and so SNR if it is limited by technical, probe beam noise (see below), which is often the case. The pumping rate is related to the pumping power. If we assume that 1.5 photons are required for pumping one atom (see previous discussion), for a cell containing N atoms, the power needed to achieve a given pumping rate R is: $P=1.5\hbar\omega NR$. For the specific case $R=R_{SD}$ for a typical spin-destruction rate of 45 s^{-1} [see Alred et al 2002] in a cell containing $N=8\times10^{14}$ atoms, $P=14$ mW. Various losses, including the reflection by the cell walls and optics, and some pumping efficiency factors would set the requirement above 20 mW for the considered case. If we have the power below this value the magnetometer signal will be below optimal value. (Here is one reason that lamps, which for a needed band have power below 1 mW, are not optimal for pumping SERF magnetometers.) In some applications the bandwidth has to be increased, so even higher pump power will be needed. To have some room for optimization for a single cell of the size 8 cc power on the order of 50 mW is needed. However, this is only a rough estimate, and each situation has to be analyzed separately, and it can be done using similar arguments. For example, the high-density rf magnetometer which relies on light narrowing and the condition $P_z\to1$ (to be discussed later), requires much higher power. The optimization condition is $R\sim\sqrt{R_{SD}R_{SE}}$, which in experiment of (Savukov et al., 2005) was about 2000 s^{-1}. This value is much larger than the value 45 s^{-1} of the optimized SERF magnetometer.

Many semiconductor lasers can provide enough power for the SERF magnetometers. However, multi-channel operation, important for magnetoencephalography (MEG) and magnetocardiography (MCG) applications, requires much higher power, on the order of 1W or more. This can be achieved with systems that have laser amplifiers or arrays of laser diodes.

While any diode laser with the required wavelength and power can be used, for best sensitivity additional requirements such as laser stability, single-frequency operation, and the absence of mode-hops have to be satisfied. In experiments with atomic magnetometers, it was discovered that so-called (distributed feedback) DFB lasers are almost ideal. These lasers are quite a novelty, with US patent issued on June 22, 2004. They work without mode hops and have low intensity noise. However, one problem exists that these lasers need additional cooling below freezing point for reaching the D1 line wavelength of K, 770 nm. In

this respect, Rb magnetometers might have advantage for which the DFB laser is available for the D1 line without cooling. Alternative lasers based on tuning by mechanical rotation of a diffraction grating are quite unstable: they can change wavelength during experiments, can suddenly increase their intensity noise to high level, when modes jump. Another interesting laser type is VCSEL. These lasers are quite inexpensive and can perform well if the current is stable. Contrary to edge-emitter, VCSEL can operate only in a single mode. It is also possible to use apparently inexpensive lasers that are commonly found in CD players that have wavelength matching the Rb D2 line (about 780 nm).

The central question in the theory of atomic magnetometers is about noise and sensitivity. There are many sources of noise, some of which are of fundamental nature and cannot be avoided, and other technical noises that can be reduces by careful choice of components and experimental arrangement. Fundamental sources of noise are spin projection noise, photon-counting noise, and light-shift noise. Technical noise arises due to probe beam intensity fluctuations, environment magnetic field, pump intensity and wavelength fluctuations, vibration, air flow, etc. Some sources of noise can be tested separately: the environment field noise and noise from the pump beam can be turned off by blocking the pump beam. The residual noise in the magnetometer signal is frequently called the probe beam noise. The probe beam noise is due to intensity fluctuations of the probe beam, as well as due to wavelength instabilities and beam steering, which can occur due to vibration, temperature drifts, or air flow. This noise directly penetrates the probe beam detection photodiodes. The intensity fluctuation noise can be reduced using either a polarizing beam splitter (PBS) or with modulation methods. The PBS if well balanced has equal intensity fluctuations in its two channel and they can be removed from the signal. The subtraction level of 100 can be achieved, which is often sufficient to reach photon shot noise performance with a good laser. The alternative technique is based on the modulation of light polarization orientation, which is especially useful for detecting low-frequency (a few Hz) magnetic field. When the probe beam passes through one polarizer, a polarization angle modulator, an atomic vapor cell, and the second polarizer with polarization axis at 90 degree angle to the light polarization, the signal will be proportional to $[\theta_{\mathrm{mod}}\cos(\omega t)+\theta_{atoms}]^2$, where ω is the frequency of modulation. With a lock-in amplifier, the first harmonic of ω can be extracted, which amplitude is proportional to the light polarization rotation by atoms θ_{atoms}, i.e. the magnetometer signal. At high enough frequency of modulation, the intensity fluctuation noise from the laser or beam steering falls down, and low frequency field can be measured with high sensitivity as if the signal occurred at high frequency. With a high-quality laser that has a noise level at modulation frequency close to the photon shot noise, it can be possible to achieve shot-noise sensitivity for the detection of polarization rotation at low frequency. One drawback of the modulation technique when it is based on Faraday modulators is the requirement for oscillating field of fairly high strength, on the order of 0.01 T. This makes the design cumbersome. Other options based on a photo-elastic modulator can be chosen to avoid this problem. It is also possible to use internal properties of the atomic vapors to modulate the AM signal.

Noise due to a pump laser is also important to consider and minimize. The intensity and wavelength fluctuations of the pump laser can penetrate to the atomic magnetometer signal due to various coupling mechanisms. One such a mechanism is light-shift. Light shift in an

atomic magnetometer affects its signal similarly to the applied magnetic field, as we discussed earlier. The effect of light shift can be modeled with the Bloch equations which contain effective light-shift "magnetic field." The circularly polarized light of pump beam, when it is not exactly tuned to the center of the line, creates light shift field in the direction of its propagation. The change in the intensity as well as in wavelength on which light shift depends will result in the change of amplitude of the effective field, resulting in magnetometer noise. One solution to this problem developed in SERF magnetometers, which is based on the SERF signal output equation

$$S_x = S_0 \frac{\gamma B_y T_2 - (\gamma T_2)^2 B_x B_z}{1 + (\gamma T_2)^2 (B_x^2 + B_y^2 + B_z^2)}, \tag{9}$$

is to zero the x component of the field. Here x is the direction of the probe beam, z is the direction of the pump beam, and y is normal to x and z. Because the z component and the x component enter this equation as the product, zeroing of the x -component will make the magnetometer signal insensitive to the z component and hence the pump beam light shift.

At high frequency the magnetometer signal is not described by Eq. 9. Instead, the response of the magnetometer is linear to small oscillating B_x and B_y fields and the magnetometer exhibits resonance which is the function of the applied B_z field. Light shift from the pump laser, does not enter directly into the signal, but merely changes resonance frequency. Thus if there are no large oscillating fields the rf magnetometer will be immune to light shift fluctuations of pump beam. However, it is not immune to the probe beam light shift fluctuations, which is equivalent to B_x noise. Thus apart from noise that can be directly seen in the detection system arising from probe beam intensity fluctuation, addition noise with characteristic ringing of AM magnetic resonance (because it is capable of exciting the spin resonances), can be present due to these fluctuations.

Environment field noise can be reduced by magnetic shielding and with gradiometers. Vibration noise can be minimized by building magnetometes on optical tables that are floated. To achieve best sensitivity, many noise reduction strategies are combined, and the magnetometers become state-of-the-art.

3. Spin-exchange free atomic magnetometer

Among various atomic magnetometers, the so-called spin-exchange-relaxation-free (SERF) magmetometer introduced by Princeton group have the highest sensitivity at low frequency for a small cell size. (In general, for comparison, it necessary to specify the size, because many magnetometers can improve their sensitivity with the size as $1/V^{1/2}$, where V is the active volume of the magnetometer.) The absence of relaxation from SE collisions is the key to the high sensitivity of SERF magnetometers. In non-SERF magnetometers when the density of vapor is increased to increase the number of atoms and naively reduce fundamental spin-projection noise, which scales as $1/\sqrt{NT_2}$ or other noises, the width of magnetic resonance $1/T_2$ dominated by SE collisions also increases and sensitivity does not improve. However, in the SERF regime, the opposite happens: with the density increase, the resonance width falls down dramatically and reaches a very small value, which is determined by spin-destruction collisions rather than by SE collisions. The situation looks

like SE is completely turned off. Because SE cross sections in many alkali-metal atoms are quite large (about 10^{-14} cm^{-2} for K, Rb, Cs) and greatly exceed those of spin-destruction collisions (by 4 orders in K, 3 orders in Rb, and 2 orders in Cs), the suppression of SE broadening leads to dramatic decrease of resonance width and improvement in sensitivity.

Although the SERF regime can be achieved at low densitities, the most beneficial densities are on the order of 10^{14} cm^{-3}. To achieve such densities the heating of alkali cells to relatively high temperatures is needed. Potassium cells require heating to about 180°C, Rb to 150°C, and Cs to 120°C. Thus one drawback of the SERF regime is relatively high temperature of operation requiring building ovens. Initially ovens of SERF magnetometers were based on hot air flow to avoid any magnetic field noise, and their design was quite cumbersome. The power efficiency of heating is also very low, with power on the order of 1 kW required. Apart from this, the air flow is arranged with an inconvenient hook-up to compressed air outlet. More recently, electrical oven designs were introduced for SERF magnetometers. While electrical current produces significant magnetic noise and can disorient atomic spins in the magnetometer, there are several ways to deal with it. The simplest method to reduce this noise is to turn off the power during measurements. While the noise becomes quite small with power off, the measurement is not continuous, which is probably the major drawback of the method. The interruptions also lead to periodic temperature variations which cause correlated variations of the AM signal. The heater element has to be chosen carefully to avoid ferromagnetic and highly conductive materials, which can cause field distortions and noise. In general, with the solution of these problems the electric oven design will be invaluable in out-of-the-lab applications where power consumption and portability are at premium.

Potassium SERF magnetometers set the record of the sensitivity, but from the comparative analysis of the noise (practical and fundamental) of SERF magnetometers for different alkali-metal atoms, which is dominated often by technical noise, it can be found that they can be used with similar results. The ratios of fundamental noise that scale as $1/Rsd^{1/2}$ in the sequence of K,Rb, Cs are about 1:3:10 for the corresponding approximate ratios of the SD rates R_{SD} 1:10:100, and even the least sensitive Cs SERF magnetometer has fundamental noise on the order of 0.1 $fT/Hz^{1/2}$, much lower than the best sensitivity level 0.5 $fT/Hz^{1/2}$ demonstrated. While the Cs SERF magnetometer is less sensitive than K fundamentally, Cs SERF requires lowest temperature of the operation and in some applications where the distance between the cell and the measured object has to be minimized, the Cs AM magnetometer will have great advantage. It can operate in the temperature range 100-140°C, and it is much easier to implement thermal insulation for these temperatures than those used in the potassium SERF magnetometer. The sensitivity of Cs SERF magnetometer has been measured in Ref. (Ledbetter et al., 2008a), and the advantage of low temperature was used for the detection of NMR in a microfluidic channel with a Cs SERF based on a microfabricated cell in Ref.(Ledbetter et al., 2008).

One important motivation for developing atomic magnetometers is owing to applications which have to be done outside the lab. In such applications, portability, small weight, low-power consumption, and vibration stability are highly desirable. The most sensitive SERF magnetometer (Kominis et al., 2003) was implemented on a special non-magnetic optical table with a multi-layer mu-metal shield reducing the ambient magnetic field by a factor of 1 million and due to the complexity of experimental arrangement and high price, such

magnetometers would have only limited use, in the lab with the aim to demonstrate highest possible sensitivity or in fundamental experiments. For external applications the design has to be simplified and miniaturized, and for successful commercialization, the price also has to be greatly reduced.

With the goal of commercialization of AMs in mind, a NIST group has been working on the micro-fabrication of miniaturized atomic vapor cells motivated also by miniature atomic clock applications (Knappe et al., 2005). The NIST group showed that the clock package can be adapted to magnetic field measurements with sensitivity of 50 $pT/Hz^{1/2}$ at 10 Hz. The clocks or the magnetometer modules consisted of many layers of various functional components: lasers, filters, lenses, quartz waveplates, ITO heaters, atomic cells, and photodiodes. The components, thin wafers, were stacked on the top of each other to form a compact assembly. Although the demonstration of a miniature AM was a real breakthrough in the magnetometer technology, the performance of the first microfabricated magnetometer was not optimal. One reason of low sensitivity was that this magnetometer was not configured as the SERF magnetometer. However, in a following experiment, a microfabricated atomic cell was tested in the SERF configuration in the SERF regime, and dramatic improvement in sensitivity, almost 1000 times, to the level of 65 $fT/Hz^{1/2}$ was achieved [Shah et al 2007]. According to fundamental noise analysis, even higher sensitivity should be possible. One problem with microfabricated cells is that they have significant spin-destruction rate due to diffusion to the walls, so linewidth is much greater than in larger-cell SERF magnetometers. Perhaps in future if high-temperature coating is developed, the diffusion to the wall can be reduced and sensitivity of microfabricated SERF magnetometer can receive further boost.

In parallel, at Princeton small-scale magnetometers (quite larger than the microchip type) have been created and sensitivity on the order of a few $fT/Hz^{1/2}$ has been demonstrated (result is not yet published). Thus probably by converging these two approaches of NIST and Princeton groups, both inexpensive and highly sensitive magnetometers can emerge soon. The commercialization of this magnetometer will be important in many applications based on sensitive and portable magnetic-field measurements.

4. "SERF magnetometer" in non-SERF regime

The SERF magnetometer is a great advance in magnetometer technology. However, the operation in the SERF regime is limited in a frequency range and in the range of ambient fields. Thus a question arises about the performance of the "SERF magnetometer" – or high-density magnetometer with the arrangement of pumping and probing as well as of other elements similar to the SERF magnetometer– outside the SERF regime; in particular, about how sensitivity changes with a frequency and applied field. The investigation of the non-SERF regime of "the SERF magnetometer" was done in Ref. (Savukov & Romalis, 2005), which resulted later in discovery of rf magnetometer (Savukov et al., 2005) and rf-based scalar magnetometer (Smullin et al., 2009). One characteristic feature in operation outside the SERF regime is the effect of SE collisions on the magnetic resonance of the magnetometer. As we mentioned SE collisions have much higher cross section than SD collisions, and the broadening due to SE collisions can be on the order several kHz for typical temperatures of vapors used in SERF magnetometers, exceeding orders of

magnitude a typical SERF bandwidth of several Hz. Because the bandwidth and the signal amplitude are inversely related in the AM, the bandwidth investigation is very important for the analysis of the sensitivity. The bandwidth of high-density magnetometers and the broadening due to SE was investigated in detail (Savukov & Romalis, 2005) experimentally and numerically by solving the DM equation.

Typically, the SERF magnetometer is operated with all fields close to zero, and the magnetometer has its frequency sensitivity profile similar to that of the first-order low-pass filter, with the bandwidth equal to the width of the magnetic resonance. The profile has the shape of Lorentzian centered on zero frequency. When the frequency of the measured field f is outside the bandwidth of the magnetometer, the signal decreases as 1/f. So SERF magnetometer loses its sensitivity very quickly beyond several bandwidths, 10-100 Hz. The sensitivity can be partially restored if a bias field is applied to tune the Zeeman resonance of the magnetometer to the applied field frequency. However, the applied bias field leads to the additional broadening arising from SE collisions. This also means that the operation goes outside the SERF regime. SE broadening increases first quadratically with the bias field, and then the dependence becomes more complicated, although monotonous. Eventually the resonance width reaches the maximum at high field at low pumping rate, which is $R_{SE}/8$ for K and or on this order for other alkali-metal atoms. The SE broadening depends not only on the bias field but also on the spin polarization or pumping rate. With high pumping rate, it is possible to increase polarization and significantly suppress SE broadening via the process of light narrowing. Because pumping leads to additional spin-destruction, the pumping rate cannot infinitely reduce the width of the magnetic resonance, and the trade-off between SE broadening and pump spin-destruction broadening exists. Light narrowing in more detail will be discussed later with regard to the operation of rf magnetometer where this effect is essential for improving sensitivity.

The transitions between Zeeman levels are excited with the change of magnetic number by 1, which is due to the term $\gamma \mathbf{J} \cdot \mathbf{B}$. Although there are many hyperfine sublevels, at low field the splitting is the same between them and multiple magnetic resonances collapse into a single resonance. In this case the Bloch equations can be a good description for spin dynamics (in the SERF regime and outside the SERF regime when excitation field is small) because the behavior of the system is similar to that of electron ½ spin. The only difference is in the presence of the so-called slow-down factor, which depends on the hyperfine level distribution (spin-polarization) and density of atoms. It was studied in detail in Ref. (Savukov & Romalis, 2005). In the K atomic vapor of high density at low field, the slow-down factor ranges from 4 to 6, which can be shown analytically using the assumption of the ST distribution. The maximum slow-down factor is reached for equal distribution over all hyperfine sublevels (small polarization limit, infinite ST), and the minimum factor is reached when only the stretched state M=I+1/2 is occupied (100% polarization, or zero ST). When the vapor density is not very high, the ST distribution is no longer enforced by SE collisions, so it is possible to create an arbitrary distribution of states; then slowing down factor can be made arbitrary large, though it is not of practical interest for magnetometers.

The case when the SE rate dominates other rates in the atomic spin system, including the rate of spin precession, is most simple for analysis. However, in practical situations Zeeman precession rate can exceed the SE rate. One consequence of this is that different Zeeman

components can decouple in their motion. In particular the lower hyperfine components and the higher hyperfine components can evolve independently. Then SE collisions will "try" to bring these components into coherent motion causing relaxation.

For strong enough field, the Zeeman splitting between different levels can also become substantially unequal, and multiple magnetic resonances can be observed if the distances between them exceed the resonance widths. This can happen in the Earth field in atomic cells with low pressure of buffer gases and anti-relaxation coating. One consequence of these multiple resonances is that a magnetometer based on measurements of the position of this resonances (the field and the position are almost linearly related) will have heading error, that is the signal at a given modulation frequency will depend not only on the field strength as would be expected for a true scalar magnetometer but also on the direction. Thus the signal of the AM exposed to a large ambient field, such the Earth field, will fluctuate when its orientation changes and this can be a problem in mobile applications.

In the non-SERF regime, the SE broadening can reach levels of several kHz for typical SERF magnetometer operating temperatures. Good understanding of SE effects is essential for designing sensitive magnetometers at arbitrary frequency. For example, the SE broadening can be suppressed with light narrowing. Light narrowing was discovered and explained in Ref.(Appelt et al, 1998 & 1999). In very simple terms, light narrowing can be explained as follows. The SE broadening occurs due to the collisions between oppositely precessing spins of F=I+1/2 and F=I-1/2 hyperfine levels. Strong pumping populates the majority of atoms into the stretched state (F=I+1/2, M=F) and the number of atoms in the lower manifold (F=I-1/2) is small. Thus there will be not many SE collisions between oppositely precessing groups and relaxation due to SE will be suppressed. More detailed explanation is provided in Refs.(Appelt et al., 1998; Savukov & Romalis, 2005; Savukov et al., 2005) where also equations are given for calculations of light narrowing. In magnetometer experiments, light narrowing leads to more than 10 time reduction in bandwidth and similar improvement in magnetic field sensitivity because in practice it is limited by probe beam noise. Although high pump rate can suppress SE broadening completely, it also broadens resonance, more or less linearly with power, so there is an optimal rate to minimize the bandwidth and to maximize sensitivity. In Ref. (Savukov et al., 2005) it was found that the transverse relaxation rate or bandwidth are related to the magnetometer parameters as

$$T_2^{-1} = \frac{R}{4} + \frac{R_{SE}R_{SD}}{R} G(\omega_0, R_{SE}) \tag{10a}$$

$$G(\omega_0, R_{SE}) = \mathrm{Re}\left[\frac{R_{SE} + 4i\omega_0^2 / \pi\nu_{HF}}{5R_{SE} + 8i\omega_0^2 / \pi\nu_{HF}} \right] \tag{10b}$$

Here ω_0 is the spin precession frequency and ν_{HF} is hyperfine frequency. This equation is derived for atoms with I=3/2. In the case of precession frequency below the MHz range, $T_2^{-1} = \frac{R}{4} + \frac{R_{SE}R_{SD}}{5R}$ and the optimized pumping rate leads to the following minimal bandwidth: $(1/T_2)_{\min} = (R_{SE}R_{SD}/5)^{1/2}$. This width is much smaller than spin-exchange broadening in no light narrowing regime, $R_{SE}/8$, because $R_{SD} << R_{SE}$, about 10,000 times in

potassium. The light-narrowing factor, which is the ratio of the minimal width for the optimal pumping rate and the maximum width without light narrowing, is $K = (5R_{SE} / R_{SD})^{1/2} / 8$. If the SD rate is dominated by K-K collisions, the condition that can always be achieved at high enough density of alkali-metal atoms, then $K = (5\sigma_{SE} / \sigma_{SD})^{1/2} / 8$, where σ_{SE} and σ_{SD} are spin-exchange and spin-destruction cross sections. Potassium has $\sigma_{SE} = 1.8 \times 10^{-14}$ cm² and $\sigma_{SD} = 1 \times 10^{-18}$ cm², so the maximum light-narrowing factor is $K_{\max} \approx 37$.

Tuning to resonance and light narrowing are two main features of high-density rf atomic magnetometers. Another interesting feature is that laser noise, as well as many other technical noises, goes down with frequency, so the rf AM can be more sensitive than the SERF magnetometer, at least in terms of real experimental noise performance. Fundamental limit of the SERF might be by several orders better, but the rf magnetometer can approach its fundamental limit closer while SERF will be by far dominated by technical noise. The fundamental noise of the rf magnetometer has been investigated in Ref. (Savukov et al., 2005). After optimization of various parameters, such as the pumping rate and the probe laser intensity, this noise can be expressed in terms of fundamental quantities of atomic vapors, such as SE and SD cross sections:

$$\delta B_{\min} = \frac{2}{\gamma}\sqrt{\frac{\bar{v}[\sigma_{SE}\sigma_{SD} / 5]^{1/2}}{V}(1 + \frac{1}{4\sqrt{\eta}})}\ , \tag{11}$$

where $\bar{v}$ is the mean thermal velocity of K-K collisions. For a typical photodiode quantum efficiency $\eta = 50$ % and a cell active volume $V = 1$ cm³ cell, the optimized fundamental magnetic field sensitivity is about 0.1 fT/Hz$^{1/2}$.

Because the rf magnetometer sensitivity exhibits resonance behavior with resonance frequency being a function of the applied DC magnetic field, this magnetometer can be converted to a scalar magnetometer by applying an rf modulation field near resonance frequency. One advantage of this approach is that the magnetometer can be used in the Earth-field environment, without mu-metal shielding or field compensation, unlike SERF. In the Earth field, the resonance frequency is about 350 kHz (I=3/2 atoms). Small variations in the Earth field can be readily observed as the shifts in the resonance. The in-phase and out-of-phase responses near the magnetic resonance have absorption and dispersion Lorenzian dependencies on frequency. It is convenient to use the dispersion component. Then the signal of the scalar magnetometer is proportional to the deviation of the field from the resonance condition. The lock-in amplifier can be used to convert DC magnetic field changes to the high-frequency rf magnetometer signal. The sensitivity to the DC field is determined by the slope of the dispersive component. The slope of the rf magnetometer was investigated in upcoming paper about scalar magnetometers (Smullin et al., 2009). Because the signal initially grows with the rf field excitation amplitude and then falls off, the optimal excitation amplitude exists. The fall off happens due to broadening of magnetic resonances, which consists of the conventional broadening that can be explained with the Bloch equations and the broadening due to SE collisions. The fundamental limit of the sensitivity of the scalar magnemeter can be derived from that of rf magnetometer in which the effects of large-excitation amplitude broadening are incorporated. Due to the additional SE

broadening at the large excitation amplitude required for maximum sensitive, the fundamental noise of the scalar magnetometer has different dependence on the SE and SD rates than the rf magnetometer. The scalar magnetometer fundamental noise is mostly determined by the SE rate, while the rf magnetometer has $[\sigma_{SE}\sigma_{SD}/5]^{1/4}$ dependence. As the result, the performance of the scalar magnetometer is expected to be quite similar for different alkali-metal atoms. Thus it can be beneficial to use other than K alkali-metal atoms requiring lower cell temperatures.

5. Applications of ultra-sensitive magnetometers

Research on atomic magnetometers is strongly motivated by many current and potential future applications. Among such applications, MEG is probably the most invaluable because no other device than the atomic magnetometer can rival low-Tc SQUIDs in sensitivity at low frequency, in the range of interest to MEG:

- MEG

History of MEG begins in 1968 when the first magnetic recordings of brain activity were registered with a Faraday coils (Cohen, 1968). Although the sensitivity of the coils in the initial demonstration was quite low, soon significant improvement was achieved when the coil was replaced with a SQUID magnetometer (Cohen, 1972). Later on, multi-channel systems have been developed to enable practical MEG source localization. Such systems became the basis for MEG research and clinical applications. However, the cost of multi-channel systems, of their maintenance, and of magnetically shielded rooms required for MEG measurements has been very high, restricting the clinical and research applications of this exciting technology. Consequently, some research has been done in the direction of cost reduction. For example, SQUID gradiometers were tested that could reduce ambient noise 1000 times to eliminate the requirement of expensive high-quality multi-layer shielded rooms. Some other ideas were tested, such as noise suppression based on open superconducting shield and reference channels (Volegov et al., 2004). However, until recently all practical MEG systems had been based on SQUIDs that required liquid helium supply, which is the major drawback.

Alternatively, MEG systems can be based on atomic magnetometers and requirements for cryogens can be eliminated. Recently, it was demonstrated that a SERF magnetometer can be successfully used for the detection and imaging of brain activities (Xia et al., 2006). Moreover, it was argued that a commercial multi-channel system can be built at a fraction of cost of a multi-channel SQUID system, so not only the AM MEG system would be more convenient in operation it would be less expensive as well. An inexpensive multi-channel operation is possible because a large atomic cell filled with a buffer gas can independenly measure magnetic field in different locations. Thus instead of building many separate magnetometers, it is sufficient to build a few large atomic cells to realize hundreds of channels. In Ref. (Xia et al., 2006) it was also demonstrated that a low cost shield can be designed for lying position consisting of mu-metal cylinders. With all these features, overall cost reduction is expected quite significant to make AM MEG system commercially viable and to extend the applications of the MEG method in research and hospitals. However, the currently demonstrated design is not suitable for building a full-head MEG system and requires further investigation.

Owing to rapid progress in AM technology and its novelty, it has to be noted that some even recent review books contain outdated notions about AMs with regard to MEG applications. For example, it is stated [see p. 273, (Clarke & Braginski, 2006) or (Wikswo, 2004), the original source] that one of the difficulties with atomic magnetometers in MEG applications is that they must be operated with a shielding factor about 10^4 times larger than that of magnetically shielded rooms currently used for biomagnetic measurements. This conclusion was drawn from the fact that shielding factor in Ref. (Kominis et al., 2003) was on the order of 10^6, but this was not essential. Actually, it was shown in a different paper (Seltzer & Romalis, 2004) that the SERF magnetometer can operate even in unshielded environment, if due field compensation is provided with a system of coils. Moreover, it was shown that with the gradiometric noise reduction technique based on multi-channel detection a relatively inexpensive shield can be used to conduct MEG experiments (Xia et al., 2006). Another outdated statement was about greater difficulty in thermal insulation of the hot oven, heated to 180°C, from the head compared to that of cryogenic systems such as SQUIDs. However, this problem was solved as well in Ref. (Xia et al., 2006). In addition to effective thermal insulation, a water cooling pad was added to make the subject comfortable during MEG sessions. The thermal insulation measures did not increase much distance from the sensor to the head or sources of the brain activity compared to that of the MEG SQUID Dewar. With regard to greater magnetic noise of the hot oven compared to that of the cold Dewar (Wikswo, 2004), it is the fact that the hot oven made of non conductive and non magnetic material does not create any magnetic noise, while in helium Dewars conductive materials are used for reflecting IR radiation to achieve minimal helium consumption, and such conductive materials produce significant noise.

- Fundamental experiments

Another possible application of AMs where high sensitivity is in demand is in fundamental physics. An example of such an application is the measurement of electric dipole moments (EDM) of atoms. There are several schemes for EDM experiments. The basic idea is to apply a strong electric field and to measure with high sensitivity a weak magnetic field arising due to EDM. Because the hypothetical atomic EDMs are extremely small, it is necessary to use sensors of highest sensitivity. Some schemes are based on unique properties of atomic spins and such experiments cannot be done with arbitrary magnetic sensors. Others do not necessarily need atomic magnetometers, and low-T_c SQUIDs can be used as well. A comprehensive review of EDM research is given in a book by Khriplovich and Lamoreaux (Khriplovich & Lamoreaux, 1997). Atomic magnetometers can be also used in other fundamental experiments such as the setting limits on CPT violation (Kornack & Romalis, 2002).

- NMR and MRI

High sensitivity of atomic magnetometers can be important for applications in unconventional low and ultra-low field (ULF) NMR and MRI. One motivation for exploring ULF MRI is that it is not based on bulky and expensive superconducting or permanent magnets and many applications supplemental to conventional MRI can be developed. For example, it is possible to combine MEG and MRI (Zotev et al., 2008) to reduce the corregistration error, or make a portable and inexpensive MRI scanner at a fraction of the

cost of conventional MRI machines. Such scanners can lead to wider spread of MRI diagnostics around the world. Normally in NMR/MRI simple pick-up coils are used, but the coils, which output signal according to Faraday's law is the time derivative of the magnetic flux, loose sensitivity at low frequency and do not perform well in the ULF regime. Apart from this, the polarization of NMR and MRI spins is also weak in this regime. On the other hand the standards of MR imaging are set very high with resolution on the order of 1 mm and SNR on the order of 30, setting demands on the sensitivity.

To enhance a weak NMR signal in the ULF regime, the method of prepolarization was proposed (Macovski & Conolly, 1993). In this method, relatively large field (whichever is practical to generate with a coil) is applied to polarize protons or other nuclear spins and is turned off during the NMR/MRI measurements. The process is repeated many times. With prepolarization method, the NMR signal is enhanced more than 1000 times compared to that would be generated in microTesla fields at which MRI enconding and readout are actually carried out. One advantage of the ULF readout and encoding is that gradients arising from the ULF coil are quite small and no shimming is necessary. Still even with prepolarization enhancement the SNR and resolution are quite inediquate if simple pick-up coils are used at low frequency, and some solution of this problem is necessary. One solution is to replace the coil with SQUIDs or AMs to achive additional gain in sensitivity. ULF MRI with SQUIDs is now a conventional way to do ULF MRI. For example, recently an airport security scanner have been built and tested based on a multi-channel SQUID detector. However, in all low-Tc SQUID applications the main drawback the requirement for cryogenics exists. The alternative solution to avoid cryogenics can be an atomic magnetometer.

The most potentially useful AM magnetometer for MRI applications (Savukov et al., 2007) is the high-density rf atomic magnetometer (Savukov et al., 2005) discussed in this chapter which not only has very high sensitivity (fundamental limit about 0.1 $fT/Hz^{1/2}$ for 1 cm^3 cell and practical noise was demonstrated 0.2 $fT/Hz^{1/2}$) but also has sufficient bandwidth, on the order of 1 kHz which is needed in MRI detection. The minimum bandwidth for efficient scanner is estimated as the product of tissue relaxation rate and the number of pixels in readout direction.

The demonstration of MRI with AM suitable for in situ imaging is the important step in the direction of developing non-cryogenic ULF-MRI system, which was done in Ref. (Savukov et al., 2009). The achieved sensitivity was on the order of 10 $fT/Hz^{1/2}$, but further significant improvement of the sensitivity is possible. Even without much modification of the system with which the demonstration was done the sensitivity on the order of 1 $fT/Hz^{1/2}$ can be achieved just by raising frequency from 3 kHz to 30 kHz, and with ultimate optimization the sensitivity limits on the order of 0.1 $fT/Hz^{1/2}$ are possible, which would make the MRI system suitable for clinical applications. This can be inferred from the scaling arguments given in Ref. (Savukov et al., 2009).

- Other potential applications based on similar sensitivity as low-Tc SQUIDs

There are many other potential application of AMs which can be developed following pioneering work on low-Tc SQUID applications. In biomedical imaging AMs can be applied to multi-channel MCG imaging. Since heart anomalies are among leading causes of death, their diagnostic is extremely important, and AM MCG can become a invaluable tool for

saving millions of lives. Multi-channel MCG provides reach information on electrical activities in the heart non-invasively, and hence this modality can be crucial for revealing heart anomalies and the analysis of their localization. In addition to biomedical applications, AMs can be also used in submarine detection, geology, archeology, military applications, and many other fields as we have already discussed in the introduction. However, currently, high-sensitivity AMs are not available commercially, and this is the main impediment for applications. We expect that in the near future the situation will dramatically change, so all these applications will receive a significant boost.

6. Conclusion

We have considered the most sensitive atomic magnetometers based on high-density alkali-metal vapors. This chapter covered the principles of the operation of ultra-sensitive magnetometers and their applications. Among applications MEG and ULF MRI have been considered in some detail. Because low-T_c SQIUDs have been known as the most sensitive magnetometers for a long time and are still considered such by many researchers, the important conclusion from this chapter should be that atomic magnetometers can provide similar sensitivity and can be used instead of SQUIDs in their applications.

7. Literature

Allred, J.; Lyman, R.; Kornack, T. & Romalis, M. (2002). A high-sensitivity atomic magnetometer unaffected by spin-exchange relaxation. *Phys. Rev. Lett.* vol. 89, 130801.

Appelt, S.; Ben-Amar Baranga, A.; C. J. Erickson, C. J.; Romalis, M. V.; Young, A. R. & Happer, W. (1998). Theory of spin-exchange optical pumping of ^{3}He and ^{129}Xe. *Phys. Rev. A* vol. 58, p. 1412.

Appelt, S.; Ben-Amar Baranga, A.; Young, A. R. & Happer, W. (1999). Light narrowing of rubidium magnetic-resonance lines in high-pressure optical-pumping cells. *Phys. Rev. A* vol. 59, pp. 2078 – 2084.

Bell, W. E. & Bloom, A. L. (1957). *Phys. Rev.* Vol. 107, p. 1559.

Bloom, A. L. (1962). Principles of Operation of the Rubidium Vapor Magnetometers. *Appl. Optics* Vol. 1, pp. 61-68.

Budker, D.; Kimball, D. F. & D. P. DeMille, D. P. (2004). Atomic physics, an exploration through problems and solutions. Oxford Univ. Press.

Clarke, J. &Braginski, A. I. (Eds.) (2006). The SQUID Handbook. Wiley-VCH.

Cohen, D. (1972). Magnetoencephalography: detection of the brain's electrical activity with a superconducting magnetometer. *Science* vol. 175, pp. 664-666.

Cohen, D. (1968). Magnetoecephalography: evidence of magnetic field produced by alpha-rhythm current. *Science* vol. 161, pp. 784-786.

Dehmelt, H. G. (1957). *Phys. Rev.* Vol. 105, p. 1487, 1924.

Happer, W. (1972). Optical Pumping. *Rev. Mod. Phys.* Vol. 44, pp. 169-250.

Groeger, S.; Pazgalev, A. S. & Weis, A. (2005). Comparison of discharge lamp and laser pumped cesium magnetometers. *Appl Phy. B* Vol. 80, pp. 645-654.

Knappe, S.; Schwindt, P. D. D.; Gerginov, V., Shah, V.; Liew, L.; Moreland, J.; Robinson, H. G.; Hollberg, L. & Kitching, J. (2006). Microfabricated atomic clocks and magnetometers. *J. Opt. A: pure Appl. Opt.* pp. S318-S322.

Kornack, T. W. & Romalis, M. V. (2002). Dynamics of Two Overlapping Spin Ensembles Interacting by Spin Exchange. *Phys. Rev. Lett.* Vol. 89, p. 253002.

Ledbetter, M. P.; Savukov, I. M.; Acosta, V. M. & Budker, D. (2008a) Spin-exchange relaxation free magnetometry with Cs vapor. *Phys. Rev. A* vol. 77, p. 033408.

Ledbetter, M. P.; Savukov, I. M.; Budker, D.; Shah, V.; Knappe, S; J. Kitching, J.; Michalak, D. J.; Xu, S. & Pines, A. (2008b). Zero-field remote detection of NMR with a microfabricated atomic magnetometer. *Proc. Natl. Acad. Sci. USA* vol. 105, p. 2286.

Khriplovich, I. B. & Lamoreaux, S. K. (1997). CP Violation Without Strangeness: Electric Dipole Moments of Particles, Atoms, and Molecules. Springer-Verlag.

Kominis, I. K.; T. W. Kornack, T. W.; Allred, J. C.& Romalis, M. V. (2003). A subfemtotesla multichannel atomic magnetometer. *Nature* vol. 422, p. 596.

Macovski, A. & Conolly, S. (1993). Novel approaches to low-cost MRI. *Magn. Reson. Med.* Vol. 40, pp. 221-230.

McDermott, R.; Trabesinger, A. H.; Mück, M.; Hahn, E. L.; Pines, A. & Clarke, J. (2002). Liquid-State NMR and Scalar Couplings in Microtesla Magnetic Fields. *Science* vol. 295, pp. 2247-2249.

Savukov, I. M. & Romalis, M. V. (2005). Effects of spin-exchange collisions in a high-density alkali-metal vapor in low magnetic fields. *Phys. Rev. A* vol. 71, p. 023405.

Savukov, I. M. & Romalis, M. V. (2005). NMR detection with an atomic magnetometer. *Phys. Rev. Lett.* vol. 94, p. 123001.

Savukov, I. M.; Seltzer, S. J.; Romalis, M. V. & and Sauer, K. L. (2005). Tunable Atomic Magnetometer for Detection of Radio-Frequency Magnetic Fields. *Phys. Rev. Lett.* vol. 95, 063004.

Savukov, I. M.; Seltzer, S. J. & Romalis, M. V. (2007). Detection of NMR signals with a radio-frequency atomic magnetometer. *JMR* Vol. 185, p. 214.

Savukov, I. M.; Zotev, V. S.; Volegov, P. L.; Espy, M. A.; Matlashov, A. N.; Gomez, J. J.; & Kraus, R. H., Jr. (2009). MRI with an atomic magnetometer suitable for practical imaging applications. *JMR* 199, pp. 188-191.

Shah, V.; Knappe, S.; Schwindt, P. D. D. & J. Kitching, J. (2007). *Nat. Photonics* vol. 1, p. 649.

Seltzer, S. J. & Romalis, M. V. (2004). Unshielded three-axis vector operation of a spin-exchange-relaxation-free atomic magnetometer." *Appl. Phys. Lett.* Vol. 85(20), p. 4804.

Smullin, S. J.; Savukov, I. M.; Vasilakis, G.; Ghosh, R. K. & Romalis, M. V. (2009). A Low-Noise High-Density Alkali Metal Scalar Magnetometer. *Archives: physics/0611085, accepted to publication to PRA*.

Volegov, P.; Matlachov, A., Mosher, J., Espy, M. A. & Kraus, R. H., Jr. (2004). Noise-free magnetoencephalography recordings of brain function. *Phys. Med. Biol.* Vol. 49, pp. 2117-2128.

Wikswo, J. P. (2004). SQUIDs Remain Best Tools for Measuring Brain's Magnetic Field. Phys. Today Vol. 57, pp. 15-17.

Xia, H.; Ben-Amar Baranga, A.; Hoffman, D. & Romalis, M. V. (2006). Magnetoencephalography with an atomic magnetometer. *Appl. Phys. Lett.* vol. 89, p. 211104.

Zotev, V. S.; Matlashov, A. N.; Volegov, P. L.; Savukov, I. M.; Espy, M. A.; Mosher, J. C.; Gomez, J. J. & Kraus, R. H., Jr. (2008). Microtesla MRI of the human brain combined with MEG. *JMR* Vol. 194, pp. 115-120.

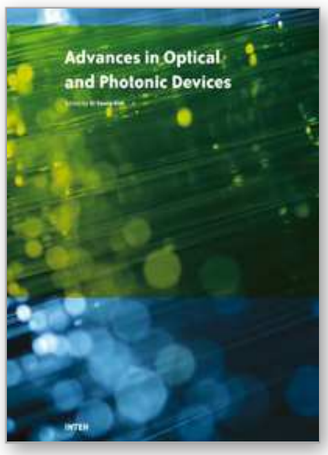

Advances in Optical and Photonic Devices

Edited by Ki Young Kim

ISBN 978-953-7619-76-3
Hard cover, 352 pages
Publisher InTech
Published online 01, January, 2010
Published in print edition January, 2010

The title of this book, Advances in Optical and Photonic Devices, encompasses a broad range of theory and applications which are of interest for diverse classes of optical and photonic devices. Unquestionably, recent successful achievements in modern optical communications and multifunctional systems have been accomplished based on composing “building blocks” of a variety of optical and photonic devices. Thus, the grasp of current trends and needs in device technology would be useful for further development of such a range of relative applications. The book is going to be a collection of contemporary researches and developments of various devices and structures in the area of optics and photonics. It is composed of 17 excellent chapters covering fundamental theory, physical operation mechanisms, fabrication and measurement techniques, and application examples. Besides, it contains comprehensive reviews of recent trends and advancements in the field. First six chapters are especially focused on diverse aspects of recent developments of lasers and related technologies, while the later chapters deal with various optical and photonic devices including waveguides, filters, oscillators, isolators, photodiodes, photomultipliers, microcavities, and so on. Although the book is a collected edition of specific technological issues, I strongly believe that the readers can obtain generous and overall ideas and knowledge of the state-of-the-art technologies in optical and photonic devices. Lastly, special words of thanks should go to all the scientists and engineers who have devoted a great deal of time to writing excellent chapters in this book.

INTECH
open science | open minds

InTech Europe
University Campus STeP Ri
Slavka Krautzeka 83/A
51000 Rijeka, Croatia
Phone: +385 (51) 770 447

InTech China
Unit 405, Office Block, Hotel Equatorial Shanghai
No.65, Yan An Road (West), Shanghai, 200040, China
中国上海市延安西路65号上海国际贵都大饭店办公楼405单元
Phone: +86-21-62489820

Fax: +385 (51) 686 166
www.intechopen.com

Fax: +86-21-62489821

IntechOpen